COMPUTATION OF TRANSONIC VISCOUS-INVISCID INTERACTING FLOW. 1983

COMPUTATION OF TRANSONIC VISCOUS-INVISCID INTERACTING FLOW*

D. L. Whitfield†
Department of Aerospace Engineering
Mississippi State University
Mississippi State, MS 39762

J. L. Thomas††
NASA Langley Research Center
Hampton, VA 23665

A. Jameson†††
Department of Mechanical and Aerospace Engineering
Princeton University
Princeton, NJ 08544

W. Schmidt††††
Dornier GmbH
Friedrichshafen, West Germany

Abstract

Transonic viscous-inviscid interaction is considered using the Euler and inverse compressible turbulent boundary-layer equations. Certain improvements in the inverse boundary-layer method are mentioned, along with experiences in using various Runge-Kutta schemes to solve the Euler equations. Numerical conditions imposed on the Euler equations at a surface for viscous-inviscid interaction using the method of equivalent sources are developed, and numerical solutions are presented and compared with experimental data to illustrate essential points.

I. Introduction

Viscous-inviscid interaction is an important and difficult problem in transonic aerodynamics. Unfortunately, numerical solutions of the Navier-Stokes equations are not presently a practical method for routinely solving such problems due to computer resource requirements. Consequently, much research has been done and must is still going on with regard to coupling inviscid and viscous flow solvers for treating viscous-inviscid interaction. Lock[1] and Melnik[2] have reviewed interaction methods. For the most part, these methods consist of using potential flow inviscid solution methods and attached flow viscous solution methods. Inverse boundary-layer methods are being used in some instances (see Le Balleur[3] for a review) in order to include separated flow.

Computational fluid dynamics has recently matured to the point that numerical solution of the Euler equations can be considered for solving two- and three-dimensional flow problems.[4-6] Because the Euler equations can handle rotational flow, these equations offer more information and an extended Mach number range compared to the potential flow equations. There has, as yet, not been a great deal of effort devoted to coupling the Euler equations with viscous flow solvers. The work that has been done includes Refs. 7-9, where the Euler equations were coupled with a compressible turbulent inverse integral boundary-layer method[10] in order to handle rotational flow that may contain regions of separated flow. The purpose of this paper is to present further results of work involving the Euler and inverse boundary-layer equations. These results include: (1) improvements in the inverse boundary-layer method, (2) numerical experiments with regard to Euler equation boundary conditions, (3) experience using second-order Runge-Kutta schemes with various number of stages to solve the Euler equations, (4) numerical conditions imposed on the Euler equations at a surface and in a wake for viscous-inviscid interaction using the equivalent source method, (5) displacement surface versus the equivalent source method of interaction, and (6) numerical and experimental comparisons.

* This research was sponsored by the NASA Langley Research Center, Hampton, VA 23665

† Professor, Member AIAA

†† Ph.D. student on leave from NASA Langley, Member AIAA

††† Professor

†††† Supervisor, Computational Fluid Dynamics

II. Viscous Method

The viscous flow solution method is an inverse (meaning the pressure distribution is obtained as part of the solution rather than being specified as in a direct method) integral compressible turbulent boundary-layer method. This inverse method is an extension of the direct method described in Ref. 11. Both methods solve the momentum and mean-flow kinetic energy integral equations. A fourth-order four-stage explicit Runge-Kutta scheme is used to solve the inverse equations.

A distinguishing feature of the direct and inverse integral methods in Refs. 11 and 7 was that the dissipation integral

$$D = \int_0^\infty \frac{\tau}{\tau_w} \frac{\partial (u/ue)}{\partial y} \, dy \qquad (1)$$

was numerically evaluated at each streamwise location as opposed to using an empirical dissipation relation. This was accomplished by using a constant laminar plus turbulent shear stress in the region just at the wall, a Cebeci-Smith type model in the inner and outer regions, and the derivative of the velocity profile expression valid for $0 \leq y < \infty$.[7, 12] Although this placed a stringent requirement on the accuracy of the velocity profile expression, the method gave good results;[7,11] even better than finite difference methods for transonic flow over adiabatic surfaces.[11, 13]

However, the numerical evaluation of the dissipation integral at each streamwise location made this integral method relatively slow (with regard to computational time) as compared to other integral methods. The computational time was not a severe limitation for steady two-dimensional flow. However, with the extension of this method to unsteady two- and three-dimensional flow, it was desirable to eliminate the need for numerically evaluating Eq. (1) at each grid point. In this connection, Donegan [10] succeeded in correlating D, as given by Eq. (1), in terms of the local edge Mach number, shape factor, and skin friction coefficient (or shape factor and Reynolds number based on momentum thickness). Recently, Thomas[14] has made improvements in the turbulence model used in Eq. (1), particularly near the separation point, and Donegan and Thomas have improved the correlation for D given in Ref. 10. The result of using an analytical correlation as opposed to numerically evaluating Eq. (1) is an increase in speed of O(10).

III. Inviscid Method

Finite volume spatial discretization is applied to the integral form of the time-dependent Euler equations and the resulting equations were solved using second-order Runge-Kutta time-stepping schemes with various number of stages. Dissipative terms composed of a blend of second and fourth differences are used in this central difference scheme and these terms are held constant during each stage of the Runge-Kutta solution. Convergence to a steady state is accelerated by the addition of a forcing term that depends on the difference between the local total enthalpy and the freestream value of enthalpy. Convergence is also accelerated by using a local time step determined by the maximum Courant number. Far field boundary conditions are based on a characteristic combination of variables, and pressure at the wall is determined using the normal momentum relation. With the exception of the use of second-order Runge-Kutta schemes with various number of stages and frozen dissipation, the numerical method is that of Jameson, Schmidt, and Turkel.[6]

An advantage of this type of explicit scheme is that stability can be achieved for Courant numbers greater than one. By using different stage Runge-Kutta schemes, the stability region can be expanded (see Fig. 1) and the maximum attainable Courant number can be increased as shown in Table 1. Although a larger Courant number can be achieved by an increase in the number of stages, the increase in work associated with the increase in stages eventually reaches a point of diminishing returns. For example, a scheme with a small value of R (see Table 1) should probably be used in the early cycles and a scheme with a large value of R thereafter. Numerical experiments indicate that the four-stage scheme is a reasonable compromise. The use of a second-order accurate scheme in time as compared to a fourth-order scheme as used in Ref. 6 has the advantage of requiring slightly less storage. Also, because steady state solutions are of interest here, and because no noticeable improvement was found in the results using a fourth-order scheme as compared to a second-order scheme, the method used was the second-order four-stage scheme with a maximum Courant number of $2\sqrt{2}$.

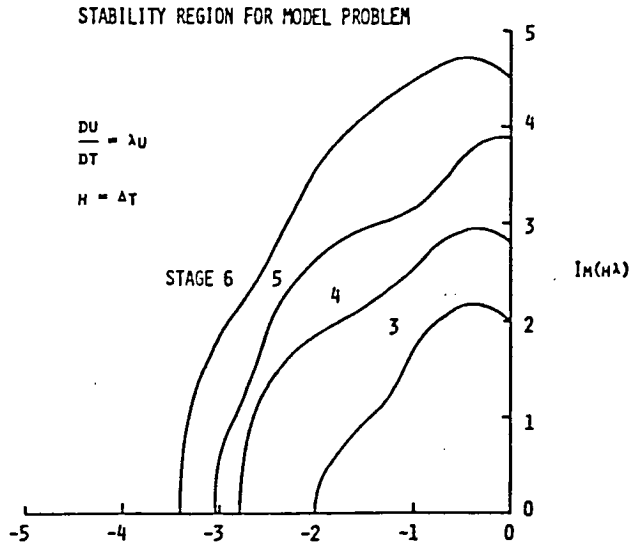

Fig. 1 Stability Region for Various Stage Second-Order Runge-Kutta Schemes

Table 1. Second-Order R-Stage Runge-Kutta (minimal storage)

$$y_{n+1} - y_n = hk_R$$
$$k_1 = f(y_n)$$
$$k_2 = f(y_n + hc_1k_1)$$
$$k_3 = f(y_n + hc_2k_2)$$
$$\vdots$$
$$k_R = f(y_n + hc_{R-1}k_{R-1})$$

R	$(CFL)_{max}$	η_1	η_2	c_i, i = 1, R - 1
1	unstable	--	--	--
2	unstable	--	--	--
3	2	.67	.50	1/2, 1/2
4	2.8	.70	.56	1/4, 1/3, 1/2
5	3.8	.76	.63	1/5, 1/5, 1/3, 1/2
6	4.5	.75	.64	1/7, 1/7, 1/4, 1/3, 1/2

$\eta_1 = \frac{CFL}{R}$ = efficiency for zero dissipation

$\eta_2 = \frac{CFL}{R+1}$ = efficiency for frozen dissipation

IV. Viscous-Inviscid Coupling

The displacement surface concept where the inviscid solution is carried out on a grid that is displaced from the actual body by the amount of the boundary-layer displacement thickness, δ^*, is the most commonly used method of viscous-inviscid interacton. This approach, however, requires that a new grid be generated after each boundary-layer solution. A viscous-inviscid interaction approach that does not require a new grid to be generated after each boundary-layer solution is the method of equivalent sources of Lighthill.[15] In this method, information from the viscous solution is used to specify a distribution of sources (either positive or negative) on the surface and in the wake, and this source distribution is used as a boundary condition in the inviscid solution. Assuming no attempt is made to align some portion of the grid with the wake, only one grid must be generated. Unlike a potential flow and boundary-layer interaction

method, an Euler equation and boundary-layer interaction method that uses the equivalent source concept requires that information be specified for the additional equations of momentum and energy. Development of the information necessary to use the equivalent source concept with an Euler equation and boundary-layer interaction method follows. This development is based on the work of Johnston and Sockol.[16] Their work is reviewed and then specific relations for the elements of the $\vec{g}$ vector of the Euler equations at a surface are obtained.

To illustrate the approach consider the steady two-dimensional Navier-Stokes equations in cartesian coordinates x, y

$$\frac{\partial \vec{F}}{\partial x} + \frac{\partial \vec{G}}{\partial y} = 0$$

and the steady two-dimensional Euler equations

$$\frac{\partial \vec{f}}{\partial x} + \frac{\partial \vec{g}}{\partial y} = 0 \qquad (3)$$

where

$$\vec{f} = \begin{bmatrix} \rho u \\ \rho uu + p \\ \rho uv \\ (e + p)u \end{bmatrix} \qquad \vec{g} = \begin{bmatrix} \rho v \\ \rho uv \\ \rho vv + p \\ (e + p)v \end{bmatrix}$$

$$e = \frac{p}{\gamma - 1} + \frac{1}{2}\rho(u^2 + v^2)$$

and u, v are velocity components in the x, y directions, and p, ρ, and e are the pressure, density and total energy per unit volume. An explicit description of the elements of $\vec{F}$ and $\vec{G}$ are not needed. Integrating Eqs. (2) and (3) with respect to y over $0 \le y \le h$, and considering the solution vectors $\vec{g}$ and $\vec{G}$ to coincide for $y > h$ (where h is taken outside the viscous region), the two integrals can be combined to obtain[16]

$$\vec{g}_o = \vec{G}_o + \frac{\partial}{\partial x}\int_o^h (\vec{f} - \vec{F})dy \qquad (4)$$

where the subscript o indicates y = 0. To avoid solving the Navier-Stokes equations, the exact solution $\vec{F}$ is represented[16] by a composite function $\vec{F}_c$, where $\vec{F}_c = \vec{F} = \vec{f} + \bar{\vec{f}} - \vec{f}_o$, and $\bar{\vec{f}}$ is a solution of the boundary-layer equations

$$\frac{\partial \bar{\vec{f}}}{\partial x} + \frac{\partial \bar{\vec{g}}}{\partial y} = 0 \qquad (5)$$

where

$$\bar{\vec{f}} = \begin{bmatrix} \bar{\rho}\bar{u} \\ \bar{\rho}\bar{u}\bar{u} + p \\ 0 \\ (\bar{e} + \bar{p})\bar{u} \end{bmatrix} \qquad \bar{\vec{g}} = \begin{bmatrix} \bar{\rho}\bar{v} \\ \bar{\rho}\bar{u}\bar{v} - \tau \\ \bar{p} \\ (\bar{e} + \bar{p})\bar{v} - \bar{u}\tau - q \end{bmatrix}$$

and τ is the shear stress and q is the heat flux. Using the composite function for $\vec{F}$, and a similar one for $\vec{G}$ (a point not mentioned in Ref. 16); Eq. (4) becomes

$$\vec{g}_o = \bar{\vec{g}}_o + \frac{\partial}{\partial x}\int_o^h (\vec{f}_o - \bar{\vec{f}})dy \qquad (6)$$

Using Eq. (6) and the definitions of $\vec{f}$, $\vec{g}$, $\bar{\vec{f}}$, and $\bar{\vec{g}}$, the following conditions on the elements of $\vec{g}_o$ are obtained.

The term $(\rho v)_o$ is given by

$$(\rho v)_o = (\bar{\rho}\bar{v})_o + \frac{\partial}{\partial x}\int_o^h [(\rho u)_o - \bar{\rho}\bar{u}]dy \qquad (7)$$

For no porosity in the boundary-layer solution $[(\bar{\rho}\bar{v})_o = 0]$

$$(\rho v)_o = \frac{d}{dx}[(\rho u)_o \delta^*] \qquad (8)$$

where δ^* is defined as

$$(\rho u)_o \delta^* = \int_o^h [(\rho u)_o - \bar{\rho}\bar{u}]dy \qquad (9)$$

The term $(\rho uv)_o$ is given by

$$(\rho uv)_o = (\bar{\rho}\bar{u}\bar{v} - \tau)_o +$$

$$\frac{\partial}{\partial x}\int_o^h [(\rho u^2 + p)_o - (\bar{\rho}\bar{u}^2 + p)]dy \qquad (10)$$

For no-slip boundary conditions for the boundary-layer solution ($\bar{u}_o = 0$), and taking the boundary-layer pressure equal to the pressure from the Euler solution at the surface

$$(\rho uv)_o = -\tau_o + \frac{d}{dx}[(\rho u^2)_o(\delta^* + \theta)] \qquad (11)$$

where θ is defined as

$$(\rho u^2)_o(\delta^* + \theta) = \int_o^h [(\rho u^2)_o - \bar{\rho}\bar{u}^2]dy \qquad (12)$$

As pointed out in Ref. 16 this approach will not provide the information necessary to obtain the pressure, and a specific approach to obtain the third element of $\vec{g}_o$ is not given in Ref. 16. The pressure is obtained here through an extension of the work of Rizzi[17] by including a surface porosity term in Rizzi's normal momentum relation. This relation is derived by Thomas[14] and the influence of including or neglecting the porosity term is demonstrated in the next section. The term $(\rho v^2 + p)_o$, therefore, is obtained by determining p_o as mentioned, and determining (ρv^2) by Eq. (8) where the density is obtained from the previous time step.

The term $[(e + p)v]_o$ is given by

$$[(e + p)v]_o = [(\bar{e} + \bar{p})\bar{v} - \bar{u}\tau - q]_o +$$

$$\frac{\partial}{\partial x}\int_o^h \{[(e + p)u]_o - [(\bar{e} + \bar{p})\bar{u}]\}dy \qquad (13)$$

Using no-slip and no porosity boundary conditions for the boundary-layer solution ($\bar{u}_o = \bar{v}_o = 0$),

an adiabatic surface $[(q)_o = 0]$, and the definition of total enthalpy ($\rho H = e + p$), Eq. (13) becomes

$$[(e + p)v]_o = (\rho vH)_o = \frac{d}{dx}\int_o^h [(\rho uH)_o - \bar{\rho}\bar{u}\bar{H}]dy \tag{14}$$

The boundary-layer method[11] was developed for an adiabatic surface with variable total enthalpy across the boundary layer that takes into account total enthalpy overshoot and nonunity Prandtl number.[18] A correlation for the integral in Eq. (14) has not been developed as yet, hence the approximation $H_o = \bar{H}$ is taken to prevent having to numerically evaluate Eq. (14) at each point. This approximation yields

$$[(e + p)v]_o = (\rho vH)_o = H_o \frac{d}{dx}[(\rho u)_o \delta^*] \tag{15}$$

which, by Eq. (8), is now simply an identity.

It is interesting to note that the combination of Eqs. (8) and (11) produce the von Kármán momentum integral equation. Hence, the results of this section can be summarized as

$$(\rho v)_o = \frac{d}{dx}[(\rho u)_o \delta^*] \tag{8}$$

$$(\rho uv)_o = u_o \frac{d}{dx}[(\rho u)_o \delta^*] \tag{16}$$

$$(\rho v^2)_o = \frac{1}{\rho_o}\{\frac{d}{dx}[(\rho u)_o \delta^*]\}^2 \tag{17}$$

$$[(e + p)v]_o = (\rho vH)_o = H_o \frac{d}{dx}[(\rho u)_o \delta^*] \tag{15}$$

and the pressure, p_o, is determined by the above mentioned extenison of Rizzi's method.[17]

V. Results

Numerical results are compared in Refs. 8 and 19 with experimental data taken on the RAE 2822 airfoil[20] that show good agreement. The computations of Refs. 8 and 19 were carried out at the geometric angle of attack, α_g, of the experiment as opposed to the corrected angle of attack, α_c, suggested in Ref. 20 to account for wall interference. Recent numerical experiments conducted to investigate the sensitivity of the solution to the grid, indicate a rather surprising sensitivity of lift to the location of the far field boundary as indicated in Fig. 2. The results in Fig. 2 were obtained by changing the location of the far field boundary, while maintaining the same far field boundary conditions[6] until there was no further change in the solution. Using the grid with the far field boundary located such that no change in the solution due to the grid would be expected, the computations for the RAE 2822 airfoil for $M_\infty = 0.730$, $\alpha_g = 3.19°$, and Re_c (freestream Reynolds number based in chord) = 6.5×10^6 were repeated. These results are presented in Fig. 3 for both the geometric angle of attach ($\alpha = \alpha_g = 3.19°$) and the corrected angle of attack ($\alpha = \alpha_c = 2.78°$) suggested by the experimentors.[20] As can be seen in Fig. 3, the agreement between the computations and the experimental data for $\alpha = \alpha_c = 2.78°$ is better than for $\alpha = \alpha_g = 3.19°$. The freestream Mach number correction of 0.004 used in Fig. 3 for the numerical solutions was that used by Lock.[1] It appears, therefore, that in view of the good agreement between numerical and experimental results obtained in Fig. 3 by accounting for the sensitivity of the far field boundary and using the corrected angle of attack, the good agreement obtained previously[8, 19] using $\alpha = \alpha_g = 3.19°$ was fortuitous. Further experimental results without wall interference, or with minimal wall interference and accurate far field measurements are needed.

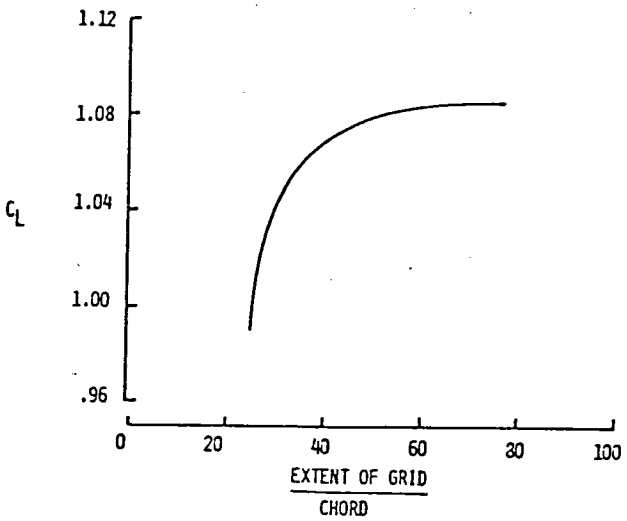

Fig. 2 Influence of the Far Field Boundary Location on the Lift Coefficient for the RAE 2822 Airfoil at $M_\infty = 0.734$ and $\alpha = 3.19°$ (Inviscid)

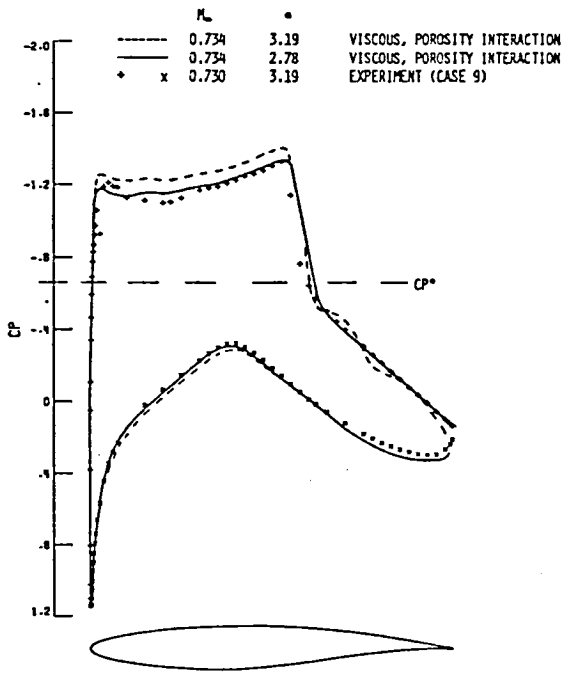

Fig. 3 Viscous-Inviscid Interaction Results for the RAE 2822 Airfoil Using Geometric (3.19°) and Experimentor's[20] Suggested Corrected (2.78°) Angle of Attack

The normal momentum relation derived by Rizzi[17] to obtain surface pressure was based on an impermeable surface. Thomas[14] has extended this work to include a permeable surface for viscous-inviscid interaction. The numerical results in Fig. 3 included this new normal momentum relation with a permeable surface. A comparison of numerical results obtained with and without the permeable surface term is given in Fig. 4 for the same flow conditions as Fig. 3. The results in Fig. 4 indicate that the influence of this term is small, although the influence the term does have is to improve the agreement with experiment slightly on the upper surface at the beginning of the shock and in the aft region of the lower surface.

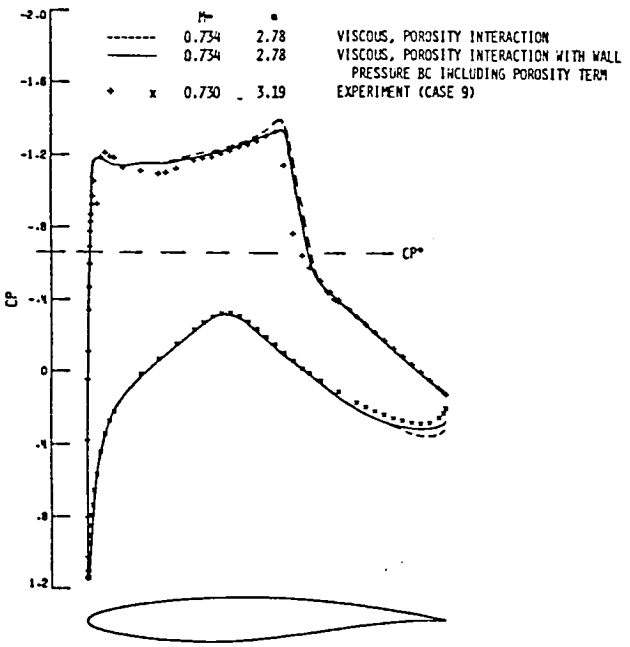

Fig. 4 Viscous-Inviscid Interaction Results for the RAE 2822 Airfoil With and Without the Porosity Term in the Surface Pressure Boundary Condition

Because the displacement surface method of viscous-inviscid interaction is the most commonly used method of calculation, a comparison is presented in Fig. 5 of the displacement surface method and the method of equivalent sources. The flow conditions used to obtain the results in Fig. 5 are the same as used to obtain the results in Figs. 3 and 4. Also, the normal momentum relation allowing for a permeable surface was used. There is some difference between the two methods of performing interaction computations as indicated in Fig. 5. The difference in shock location, for example, is of the order of the distance between grid points in this region. As mentioned, the method of equivalent sources requires that only one grid be generated, whereas, the displacement surface requires a new grid for each new boundary-layer displacement surface. The method of equivalent sources has been found the easiest to use once all the source relations are derived and coded.

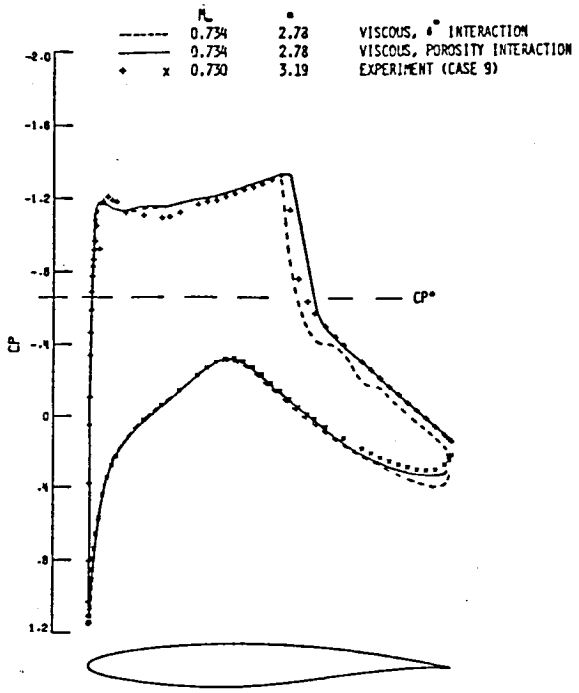

Fig. 5 Viscous-Inviscid Interaction Results for the RAE 2822 Airfoil Using Displacement Surface and Equivalent Source Methods of Interaction

VI. Concluding Remarks

The results presented involved improvements and experiences with previous work in using Euler and inverse boundary-layer equations for treating transonic viscous-inviscid interaction. Improvements in the inverse boundary-layer method included the handling of the turbulence modeling, particularly near separation, and a correlation for the dissipation integral which eliminated the need for numerical integration, and thereby reduced the computational time of the viscous solutions. Solutions of the Euler equations indicated a significant influence of the far field boundary on the lift of a supercritical airfoil with a reasonably strong shock on the upper surface. The computed lift did not change once the far field boundary was moved far from the airfoil. This observation is receiving further investigation. The use of second-order Runge-Kutta schemes with various number of stages indicated that a second-order four-stage scheme with a maximum Courant number of $2\sqrt{2}$ was a reasonable compromise for solving the Euler equations. Additional numerical surface conditions for the momentum and energy equations were developed and used in the Euler equations for the equivalent source method of viscous-inviscid interaction. Accounting for a permeable surface in the normal momentum relation used to obtain pressure produced a slight improvement in the results. Finally, numerical solutions indicated some difference between the displacement surface method and the equivalent source method of viscous-inviscid interaction, although the difference in shock location was approximately the same as the distance between grid points. The eqivalent source method is the easiest to use and requires that only one grid be generated.

The present work was carried out on a CYBER 203 in 64-bit mode with only a small portion of the code vectorized. Typical run times were 208 seconds for 1000 Euler equation cycles on a 128 x 30 grid with 16 boundary-layer solutions. Experience indicates that a similar solution obtained on a CRAY-1S requires about half this amount of time.

References

(1) Lock, R. C. "A Review of Methods for Predicting Viscous Effects on Aerofoils and Wings at Transonic Speeds," AGARD-CPP-291, 1980.

(2) Melnik, R. E. "Turbulent Interactions on Airfoils at Transonic Speeds - Recent Developments," AGARD-CPP-291, 1980.

(3) Le Balleur, J. C. "Viscid-Inviscid Coupling Calculations for Two and Three Dimensional Flows." Lecture Series 1982-04, von Kármán Institue for Fluid Dynamics, March 29 - April 2, 1982.

(4) Jacocks, J. L. and Kneile, K. R. "Computation of Three-Dimensional Time-Dependent Flow Using the Euler Equations," AEDC-TR-80-49, Arnold Air Force Station, TN, October 1980.

(5) Rizzi, A. and Eriksson, L. E. "Transfinite Mesh Generation and Damped Euler Equation Algorithm for Transonic Flow Around Wing-Body Configurations," AIAA Paper No. 81-0999, June 1981.

(6) Jameson, A. Schmidt, W., and Turkel, E., "Numerical Solutions of the Euler Equations by Finite Volume Methods Using Runge-Kutta Time-Stepping Schemes," AIAA Paper No. 81-1259, June 1981.

(7) Whitfield, D. L., Swafford, T. W., and Jackocks, J. L. "Calculation of Turbulent Boundary Layers with Separation and Viscous-Inviscid Interaction," AIAA Journal, Vol. 19, No. 10, October 1981, pp. 1315-1322.

(8) Schmidt, W., Jameson, A., and Whitfield, D., "Finite Volume Solutions to the Euler Equatons in Transonic Flow," J. of Aircraft, Vol. 20, 1983.

(9) Whitfield, D. and Jameson, A., "Three-Dimensional Euler Equation Simulation of Propeller-Wing Interaction in Transonic Flow," AIAA Paper No. 83-0236, January 1983.

(10) Whitfield, D. L., Swafford, T. W., and Donegan, T. L. "An Inverse Integral Computational Method for Compressible Turbulent Boundary Layers," in Transport Phenomena in Fluid Mechanics, Springer-Verlag, Berlin, 1982.

(11) Whitfield, D. L. "Integral Solution of Compressible Turbulent Boundary Layers Using Improved Velocity Profiles," Arnold Air Force Station, TN, AEDC-TR-78-42, December 1978.

(12) Whitfield, D. L. "Analytical Description of the Complete Turbulent Boundary-Layer Velocity Profile," AIAA Journal, Vol 17, No. 10, October 1979, pp. 1145-1147.

(13) Swafford, T. W. "Calculation of Skin Friction in Two-Dimensional, Transonic Turbulent Flow," Arnold Air Force Station, TN, AEDC-TR-79-12, April 1979.

(14) Thomas, J. L. "Viscous-Inviscid Interaction Using Euler and Inverse Boundary-Layer Equations," Ph.D. Dissertation, Mississippi State Unviersity, 1983.

(15) Lighthill, M. J., "On Displacement Thickness, " Journal of Fluid Mechanics, Vol. 4, Part 4, 1958, pp. 383-392.

(16) Johnston, W. and Sockol, P. "Matching Procedure for Viscous-Inviscid Interactive Calculations," AIAA Journal, Vol. 17, No.6, June 1979, pp. 661-663.

(17) Rizzi, A., "Numerical Implementation of Solid-Body Boundary Conditions for the Euler Equations," ZAMM, Vol. 58, 1978, pp. 301-304.

(18) Whitfield, D. L. and High, M. D., "Velocity-Temperature Relations in Turbulent Boundary Layers with Nonunity Prandtl Numbers," AIAA Journal, Vol. 15, No. 3, March 1977, pp. 431-434.

(19) Whitfield, D., Jameson, A., and Schmidt, W., "1980-81 AFOSR-HTTM-Standford Conference on Complex Turublent Flows: Comparison of Computation and Experiment," Stanford, CA, September 1981.

(20) Cook, P. H., McDonald, M. A., and Firmin, M. C. P., "Aerofoil RAE 2822-Pressure Distribution, and Boundary Layer and Wake Measurements," in Experimental Data Base for Computer Program Assessment, AGARD-AR-138, 1979.